Radiation Physics and Chemistry 222 (2024) 111788

Contents lists available at ScienceDirect

Radiation Physics and Chemistry

journal homepage: www.elsevier.com/locate/radphyschem

Computational evaluation of the bucky components influence on the estimation of normalized glandular dose in digital mammography

J. Godeli [a,*], D.M. Cunha [b], M.P.A. Potiens [c], M.E. Poletti [a]

[a] Departamento de Física, Faculdade de Filosofia, Ciências e Letras de Ribeirão Preto, Universidade de São Paulo, Ribeirão Preto, SP, Brazil
[b] Instituto de Física, Universidade Federal de Uberlândia, Uberlândia, MG, Brazil
[c] Instituto de Pesquisas Energéticas e Nucleares, Comissão Nacional de Energia Nuclear, IPEN/CNEN, São Paulo, SP, Brazil

ARTICLE INFO

Keywords:
Mammography
DgN
Bucky
Influence
Simulation

ABSTRACT

The mean glandular dose (MGD) is the most suitable dosimetric quantity used in mammography to describe the absorbed dose by the breast, although it cannot be directly acquired. Studies have provided conversion factors widely implemented in international dosimetry protocols to estimate MGD, such as normalized glandular dose (DgN). Over time, the DgN estimation was refined by considering geometric models that approach a real clinical environment, such as new anode/filter combinations, compression plate and breast models. However, there is no detailed study of how the bucky (support plate, antiscatter grid and detector) can affect the DgN estimation. A modified PENELOPE Monte Carlo code was used for DgN estimation. The irradiation geometric model was built as a complete digital mammography system, considering a homogeneous breast and different typical bucky models in commercial mammography units. Simulations were carried out for mono and polyenergetic beams considering different imaging geometries. Studies with monoenergetic beams showed that the bucky presence affected DgN mainly for higher beam energies and thinner breasts. The breast support plate was the bucky component that most affected the DgN, followed by the antis-scatter grid and finally, the image detector. Studies with polyenergetic conventional (low-energy) spectra showed that the bucky exerted a minimal influence on DgN values (less than 1.0%). For high-energy spectra, mainly employed in modalities such as contrast-enhanced digital mammography, the DgN values were more affected by the bucky, increasing by 4.8% the DgN values for a 2 cm thick breast and a W/Cu 50 kV spectrum. Bucky inclusion in computer simulations is highly recommended mainly for thinner breasts and high-energy spectra. To simplify the simulations, we confirm that a homogeneous carbon fibre block support, with thickness between 3.9 and 4.1 mm, can be used as a good substitute for a complete bucky model.

1. Introduction

The International Agency for Research on Cancer (IARC) and American Cancer Society points to breast cancer as the leading cause of cancer deaths among women, with more than 680.000 reported deaths worldwide in 2020 (Sung et al., 2021). Mammography imaging technique is currently the most suitable method for the diagnosis and prevention of cancer, although this imaging modality presents risks of radiation-induced carcinoma (Miglioretti et al., 2016). To measure this risk, Karlsson et al. (1976) proposed the estimation of the mean glandular dose (MGD). This quantity is currently the most recommended test for quality control in mammography (Dance and Sechopoulos, 2016) and is defined as the product between the entrance skin air kerma (ESAK) or exposure and a conversion factor, called by several authors as normalized glandular dose (DgN) (Stanton et al., 1984; Wu et al., 1994; Boone, 2002; Fedon et al., 2015; Nosratieh et al., 2016; Sarno et al., 2017).

Initially, simple geometric models representing clinical conditions were employed to reproduce a complete mammography environment, due to computational limitations. Dance (1990) estimated the normalized glandular dose as a function of the half value layer (HVL), considering only the homogeneous breast surrounded by a skin layer, the breast compressor and an image receptor. Subsequently, other studies have extended DgN estimates to other conventional (Wu et al., 1991, 1994; Boone, 1999; Dance et al., 1999, 2000, 2009) and high-energy X-ray beams (used in imaging techniques such as contrast-enhanced, tomosynthesis and dual-energy) (Dance, 1990; Boone, 1999; Zhang et al., 2012; Cunha et al., 2013; Dance and Young, 2014; Nosratieh et al., 2016). Further works observed the influences of the spectra

* Corresponding author.
E-mail address: juliogodeli@usp.br (J. Godeli).

https://doi.org/10.1016/j.radphyschem.2024.111788
Received 23 February 2024; Received in revised form 19 April 2024; Accepted 24 April 2024
Available online 25 April 2024

characteristics, such as tube potential, anode/filter combination and source-to-skin distance (Wu et al., 1991, 1994; Boone, 1999; Dance et al., 2000). Dance et al. (2000) proposed the *g-factor* as a correction for different anode/filter combinations, showing that the DgN values can vary up to 6.1% for a fixed tube potential. Hemdal (2011) pointed out the importance of the compression plate in glandular dose estimations. The influence of different breast models was also analysed, varying their elemental composition (Carlsson and Dance, 1992), glandular fraction, distribution and positioning of glandular tissue (Wu et al., 1991, 1994; Boone, 1999; Dance et al., 2000, 2005; Hernandez et al., 2015) and skin models (Huang et al., 2008; Sarno et al., 2017; Massera and Tomal, 2018). Breast dosimetry protocols were established in order to standardize the conversion factors. The European (Engen et al., 2013), IAEA (IAEA, 2007) and United Kingdom (IPEM, 2005) protocols are based on the conversion factors proposed by Dance and collaborators (Dance, 1990; Dance et al., 2000, 2009; Dance and Young, 2014; Dance and Sechopoulos, 2016). Over the years, Dance and collaborators expanded the conversion factors for a wide range of spectra, with different anode/filter combinations and tube potentials. Previously, the American protocol (ACR, 1999) used a method adapted from Wu et al. (1991, 1994), using a standard ACR phantom. This protocol, published in 1999, is outdated as it was developed solely for screen-film mammography. In 2018, a new ACR mammography quality control manual was published (ACR, 2018), expanding its data for digital mammography and breast tomosynthesis. This manual uses a different method, proposed by Dance and collaborators (Dance et al., 2000, 2009, 2011). Although computational simulations evolved and become more complete over the years (Sechopoulos et al., 2023), there is no detailed information on the literature on how the mammography bucky can influence DgN estimations.

The mammography bucky can be simplified as a set of three components: First, the breast support plate, which can be considered as a homogeneous plate composed of a low atomic number material, such as polymethylmethacrylate (PMMA) or carbon fibre (Dance et al., 2000; Sechopoulos et al., 2007; Massera and Tomal, 2018). Second, the antiscatter grid, containing strips with a high atomic number material, such as lead or copper, separated by an interstitial space composed of materials that allow a high photon transmission, such as PMMA or air (Dance et al., 1992; Rezentes et al., 1999; Cunha et al., 2012). Third, the image detector, which consists of a thin photosensitive material, such as caesium iodide (CsI) or amorphous selenium (aSe) (Yaffe, 2010).

This work presents a detailed study on how the mammography bucky can affect the estimate of DgN values and evaluates the bucky influence on DgN values previously tabulated on international protocols, which use homogeneous breast models. For this, computer simulations were performed by considering a complete geometric model built on a modified Monte–Carlo PENELOPE code (Salvat et al., 2009). Initially, several tests were carried out with monoenergetic beams, in order to study the direct influence of each bucky component on DgN values for different conditions, such as beam energy, configuration of each bucky component and breast thickness. Later, studies with polyenergetic beams were carried out. For this step, geometric models and simulation conditions previously established by the literature were reproduced, with and without the bucky presence, in order to evaluate how the bucky inclusion can influence the pre established DgN values in literature, on which the international mammography protocols are based on. Additionally, studies with homogeneous blocks with different thicknesses placed under the breast were carried out in order to evaluate a suitable substitute for the whole bucky simulation.

2. Materials and methods

2.1. Study of the bucky influence on monoenergetic values of DgN

2.1.1. Geometric model

The simulated geometric model was based on recommendations of the report AAPM TG-195 case III (Sechopoulos et al., 2015). Some alterations were made in order to consider a digital mammography system with all bucky components included, as shown on Fig. 1. The model includes an X-ray source, a chest wall and a compressed semicircular breast, resting on a bucky represented by a support plate, an antiscatter grid and an image detector.

All bucky components were modelled with the PENGEOM package (Almansa et al., 2021) of the PENELOPE Code, defined by means of their limiting quadratic surface. The X-ray source with a focal spot of 0.3 × 0.3 mm^2 was positioned 66 cm above the detector. A rectangular (30 × 30 × 170 cm^3) block of water represented the chest wall. The compression paddle was simulated as a PMMA block, with the dimensions similar to the detector (18 × 24 cm^2) and thickness of 3 mm (Cunha et al., 2012; Del Lama et al., 2017). The breast was modelled as an 8 cm radius semi-cylinder, with thickness from 2 to 8 cm. Its inner layer was composed by a homogeneous mixture of adipose and glandular tissues, surrounded by an outer layer of 1.45 mm thick skin tissue (Huang et al., 2008). The glandular fraction was fixed at 50%. The elemental compositions and densities of breast and skin tissues were based on the data provided by Hammerstein et al. (1979). The bucky was separated into three components: breast support plate (*BSP*), antiscatter grid (*ASG*) and image detector (*ID*). Several models of these components were considered, according to the literature (Dance et al., 1992; Rezentes et al., 1999; Massera and Tomal, 2018; Dance et al., 2000; Zhao and Zhao, 2008; Dance et al., 2009; Yaffe, 2010; Cunha et al., 2012). A cover was considered for the antiscatter grid, composed of 0.3 mm carbon fibre plus 0.13 mm polyester (Dance et al., 1992), placed on both extremities of the grid. The detectors were modelled as homogeneous plates. Table 1 shows each bucky component considered in this work. The combinations of bucky components are also described on Table 1, being based on bucky configurations present on real mammography systems.

2.1.2. Monte Carlo simulations and score quantities

The simulations were carried out using the PENELOPE code (version 2008) (Salvat et al., 2009). To obtain good accuracy in the results, the simulations were performed with 10^8 primary photons. Each run took from 150 to 600 min (processor Intel Core i7-3770k CPU @ 3.50 GHz). The minimal statistical uncertainty obtained, as proposed in AAPM TG-195, was approximately 0.1%. Monoenergetic photons from 5 to 50 keV were considered. The simulations were carried out considering an irradiation field that covered all the detector surface (18 × 24 cm^2). Both photons and electrons were followed, tracking their path until the cut-off energy of 1 keV. The electrons were tracked down since they can exert influence over fluorescent-generated photons from materials with medium and high atomic numbers.

The PENELOPE code was adapted to compute the energy (E_i) and incident angle (θ_i) of photons that reached a region of interest (A), positioned directly under the compression paddle, with area of 30 × 30 mm^2 and placed 40 mm from the chest wall (disregarding backscatter) (Dance and Young, 2014). Thus, the incident Air Kerma K_{air} was calculated, in mGy, through Eq. (1) (Sarno et al., 2017).

$$K_{air} = \sum_i \frac{E_i}{A \times cos(\theta_i)} \times \left(\frac{\mu_{tr}}{\rho}(E_i)\right)_{air} \quad (1)$$

where $\left(\frac{\mu_{tr}}{\rho}\right)_{air}$ is the air mass energy transfer coefficient. In order to simplify our simulations, we implemented analytical exponential equations on the main program, fitted to calculate the $\left(\frac{\mu_{tr}}{\rho}\right)_{air}$, in cm^2/g, based on ICRU-90 database (ICRU, 2016) considering the energies between 1 and 50 keV. The fitted equations were validated by comparing our calculations with the NIST database (Higgins et al., 1991), observing very good agreement (difference lesser them 1%) between our results and the literature.

The mean glandular dose was calculated, in mGy, by Eq. (2):

$$MGD = \sum_i \left(\frac{Eabs_i}{M \times g_r}\right) \times G \quad (2)$$

where $Eabs_i$ is the energy absorbed by the breast after each photon interaction, M is the breast tissue mass (without skin tissue), g_r is the

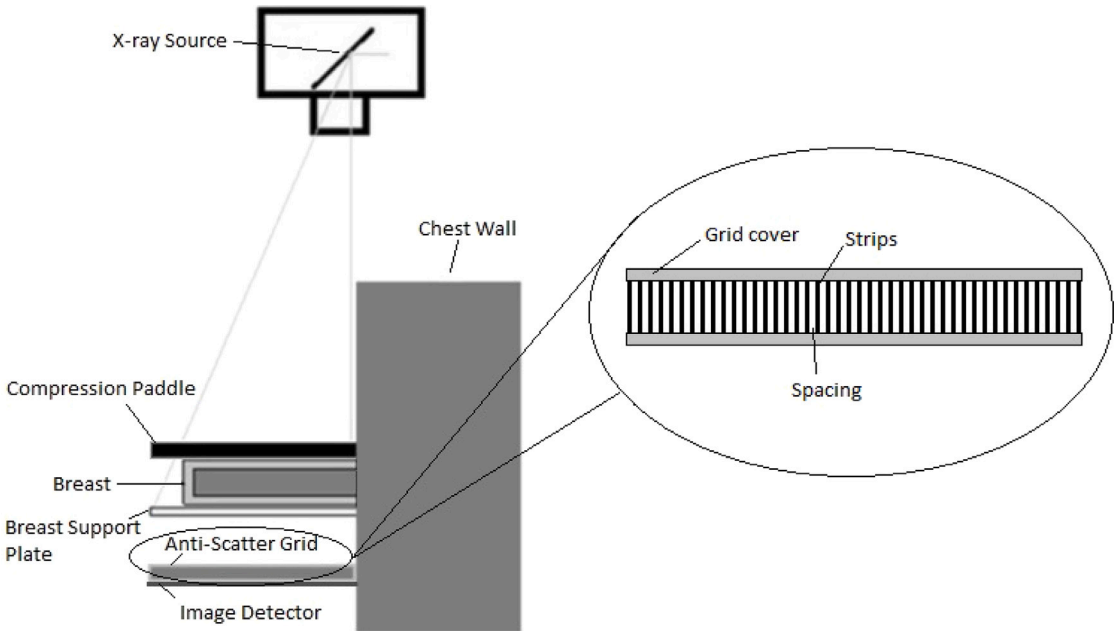

Fig. 1. Simulated geometric model (not to scale).

Table 1
Bucky components and its combinations considered in this work.

Breast Support Plate (*BSP*)				
Material		Density (g/cm2)	Thickness (mm)	Literature
Carbon Fibre		1.45	1.20	Dance et al., 2000
Carbon Fibre		1.45	2.10	This Work
Carbon Fibre		1.45	4.10	Dance et al., 2009
PMMA		1.19	2.00	Massera and Tomal., 2018
antiscatter Grid (*ASG*)				
Grid Strips	Interspace	Height (mm)	Frequency (cm-1)	Literature
Pb (Linear)	PMMA (0.3 mm)	1.50	31 lines	Dance et al., 1992
Cu (Cellular)	Air (0.64 mm)	2.40	15 cells	Rezentes et al., 1999
Image Detector (*ID*)				
Material	Thickness (μm)	Literature		
CsI	150	Yaffe, 2010 ; Cunha et al., 2012		
aSe	250	Zhao and Zhao, 2008 ; Yaffe, 2010		
Complete Bucky (*CB*)				
Combinations				Label
2.1 mm carbon fibre *BSP* + Linear *ASG* (Pb+PMMA) + CsI *ID*				*CB1*
2 mm PMMA *BSP* + Cellular *ASG* (Cu+Air) + aSe *ID*				*CB2*
2.1 mm carbon fibre *BSP* + aSe *ID*				*CB3*

breast mass glandular fraction and G is a weighting factor, proposed by Boone (1999), that estimates the energy fraction absorbed by the glandular tissue:

$$G = \frac{g_r.(\frac{\mu_{en}}{\rho})_{gl}}{g_r.(\frac{\mu_{en}}{\rho})_{gl} + (1-g_r).(\frac{\mu_{en}}{\rho})_a} \quad (3)$$

where $\frac{\mu_{en}}{\rho}$, is the mass energy absorption coefficient of glandular (gl) and adipose (a) tissues. These coefficients were estimated based on their elemental compositions (Hammerstein et al., 1979) and according the mixture rule, with values for mass energy-transfer coefficients provided by NIST (Higgins et al., 1991). These calculations were validated by comparing our values for $\frac{\mu_{en}}{\rho}$ with those provided by NIST (Higgins et al., 1991), for the adipose tissue. We observed a very good agreement (differences lesser than 1%) between our values and the literature, within the energy range considered in this work. The G-factor was estimated interaction-by-interaction (Wilkinson and Heggie, 2001).

The normalized glandular dose (DgN) was estimated, in mGy/mGy, by the following equation (Stanton et al., 1984; Wu et al., 1991; Boone, 1999):

$$D_gN = \frac{MGD}{K_{air}} \quad (4)$$

2.1.3. Simulation steps

To assess the bucky influence on DgN values as a function of the beam energy and breast thickness, simulations were performed including each bucky component step-by-step, (i) first simulating only the breast (considered as a reference), (ii) later adding the breast support plate, followed by (iii) the antiscatter grid and finally, (iv) the image detector. Simulation of the grids were conducted separately from the rest of the bucky components, due to their complex geometry, which requires a large number of objects to simulate the grid strips or cells. For the grid geometry, the grid strips were reproduced with the CLONE function of the PENGEOM (Almansa et al., 2021). Simulations were performed with photons with energies between 1 and 50 keV and incident angles between 0 and 89° from the z-axis. In order to score the transmitted, backscattered and fluorescence photons in function of the photon energy and incident angle, impact detectors were placed on top and bottom of the grid. Were assessed the characteristic photons from the radiopaque material and the overall backscatter from the whole grid, regardless of which component (cover, interstitial space and radiopaque material) the photon interacted with. The method was validated through comparison with Zhou et al. (2016) data of transmission ratios of primary and scattered photons, adapted to the

authors conditions, considering a 4 cm PMMA phantom placed above a linear grid, irradiated by polyenergetic beams (Rh-0.27 mm Cu). Our data showed very good agreement with the literature (differences lesser than 3%).

These parameters were then used as input in the main simulations of the bucky to estimate the ASG influence on DgN. As the tracked photon reached the antiscatter grid position, a series of Monte Carlo assessments were conducted. The probability of the photon transmission was estimated, according to its energy and incident angle. If the photon was transmitted, its tracking continued normally. On the other hand, if the photon interacted with the grid, the probability of backscatter or fluorescence were estimated.

For the tests analysing the image detector influence on DgN values, we considered the probability of transmission through the grid as well. Photons that backscatter from the detector surface and fluorescent-generated photons that reached the antiscatter grid position also had its transmission evaluated.

The relative influences of each bucky component on the DgN values were briefly analysed, varying their models and composition referenced in literature (Dance et al., 1992; Rezentes et al., 1999; Massera and Tomal, 2018; Dance et al., 2000; Zhao and Zhao, 2008; Dance et al., 2009; Yaffe, 2010; Cunha et al., 2012).

2.2. Comparison between polyenergetic DgN values acquired with and without the bucky presence using geometric models and simulation conditions provided by literature

To evaluate the bucky influence on DgN values tabulated on European breast dosimetry protocols (Engen et al., 2013; IPEM, 2005; IAEA, 2007), the geometric models and simulation conditions developed by Dance (1990) and Dance and Young (2014) were reproduced. The geometric model adopted by Dance (1990) consists of a semi-cylindrical breast with 8 cm radius and thickness ranging from 2 to 8 cm, surrounded by a 5 mm thick layer of adipose tissue, representing the skin. Dance and Young (2014) adopted a geometric model similar to that presented by Dance (1990), however, considering a homogeneous plate composed of 4.1 mm thick carbon fibre, positioned under the breast.

DgN values tabulated in American protocols (ACR, 1999, 2018) and vastly referenced in literature (Sarno et al., 2017; Ding and Molloi, 2017; Fedon et al., 2019) were also evaluated. For this step, the geometric model and simulation conditions proposed by Wu et al. (1994) was reproduced and studied. The geometric model adopted by Wu et al. (1994) consists of a 3 cm thick semi-elliptical breast (r_a = 9 cm and r_b = 8 cm) with a 4 mm thick layer of skin.

Dance (1990), Dance and Young (2014) and Wu et al. (1994) used their own codes to perform the simulations.

For the estimation of DgN using the geometric models of Dance (1990) Dance and Young (2014), the formalism adopted by Dance et al. (2000) was used, where it is considered: DgN = *g.c.s*. Where, *g* is the conversion factor of air Kerma to MGD, considering a breast with 50% glandular fraction, *c* is the correction factor for other breast glandularities and *s* is the correction factor for the spectrum considered.

The influence of all bucky models on the DgN values, described in Table 1, were analysed through simulations carried out with the geometric model proposed by Dance and Young (2014).

The simulations were performed using conventional and high-energy mammography X-ray beams, consistent with those used by each author. X-ray spectra were obtained for different anode/filter combinations and tube potentials through the model proposed by Boone et al. (1997). Table 2 specifies the spectra used in each geometric model.

The simulations were carried out with and without the inclusion of the bucky, being considered relevant any increase in DgN values greater than the measured uncertainty of 0.1%.

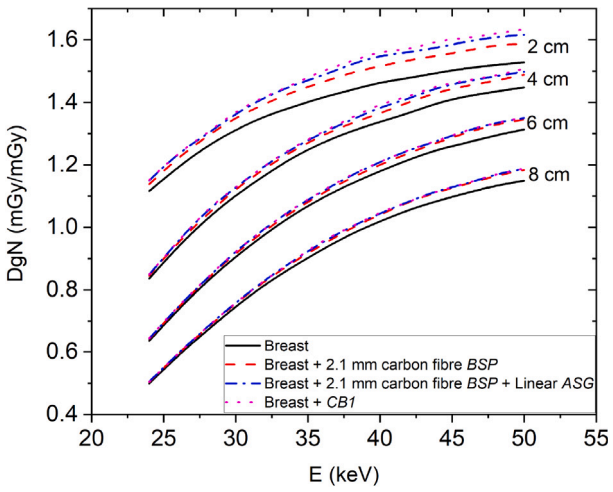

Fig. 2. DgN values as a function of the beam energy, for breasts with thicknesses varying from 2 to 8 cm, considering a addition of each bucky component.

2.3. Validation

The modification of PENELOPE code for calculating MGD values was validated through the report AAPM TG-195 case III recommendations (Sechopoulos et al., 2015). For comparison, the results of Sarno et al. (2017) were also presented alongside those found in the report (AAPM, 2015). Using the monoenergetic beam, the observed differences between our results and those of AAPM-TG195 and Sarno et al. were 0.25% and 1.11%, respectively. For the polyenergetic beam, the difference were 0.33% and 0.71%, respectively. A good agreement was observed between the simulated results in this work and the literature for both monoenergetic and polyenergetic beams, which validates the adaptation of the PENELOPE code for MGD calculations.

3. Results and discussions

3.1. Study of the bucky influence on monoenergetic values of DgN

3.1.1. Overview of the whole bucky influence

Fig. 2 shows the computed DgN values, considering a 50% glandular breast model covered by 1.45 mm of skin, positioned upon a bucky corresponding to the *CB1* configuration, as shown in Table 1. Simulations carried out with photons with energies up to 24 keV showed that the bucky inclusion had a minimal influence on the DgN values. Therefore, these results are not shown in this step.

Fig. 2 illustrates the influence of the inclusion of each bucky component on simulated DgN values, considering 2 to 8 cm thick breasts. From the figure it is observed that when the whole bucky is considered, the DgN values increase mainly for higher energies and thinner breasts. The 2 cm thick breast was the most affected by the bucky presence, showing an increase of 7% in DgN value for 50 keV beam. For this energy, the 4, 6 and 8 cm thick breasts presented an increase of 4.3%, 3.3% and 3.1% in DgN values, respectively. This reduction in the bucky influence for thicker breasts can be explained by the decrease in photons transmitted through the breast, affecting the relative contribution of the bucky region directly below the breast surface.

Additional tests were conducted with different breast models, varying their glandular fractions. Although the same trends as those presented for the 50% glandular breast were found, there was a minimal reduction on the bucky influence over the DgN with the increasing glandular fraction.

Further test were carried for a fixed 50% glandular breast and varying the skin tissue model (Massera and Tomal, 2018). The same trends and no significant differences on the bucky influence over the DgN values for all the skin models tested were observed.

Table 2
X-ray spectra used in this work to reproduce DgN values obtained in the literature.

Conventional mammographic spectra			
Anode/Filter	Tube potential (kV)	HVL range (mmAl)	Literature
Mo - 0.03mmMo + Al	20 - 35	0.25 - 0.45	Dance, 1990
Mo - Rh	35	0.44 - 0.54	Wu *et al.*, 1994
High-energy mammographic spectra			
Anode/Filter	Tube potential (kV)	HVL range (mmAl)	Literature
W - Al	40 - 50	1.00 - 2.00	Dance, 1990
W - 0.3mmCu	40 - 50	2.57 - 3.54	Dance and Young, 2014

Table 3
Relative contribution of each bucky component over DgN values. For ASG and ID, the proportion of fluorescent energy in each contribution is shown in parentheses.

Relative contribution per component (%) - CB1			
Energy (keV)	BSP - 2.1 mm Carbon Fibre	Linear ASG (% Fluorescence)	CsI ID (% Fluorescence)
24	65.8	33.7 (52.3)	0.5 (0.00)
34	62.6	23.9 (24.2)	13.5 (97.5)
42	60.3	23.8 (11.6)	15.9 (99.1)
50	62.0	26.3 (6.1)	11.2 (98.3)
Relative contribution per component (%) - CB2			
Energy (keV)	BSP - 2 mm PMMA	Cellular ASG (% Fluorescence)	aSe ID (% Fluorescence)
24	75.7	21.8 (11.0)	2.5 (91.5)
34	75.4	23.3 (3.3)	1.3 (68.6)
42	71.0	28.0 (1.4)	1.0 (42.6)
50	67.5	31.6 (0.0)	0.9 (24.1)
Relative contribution per component (%) - CB3			
Energy (keV)	BSP - 2.1 mm Carbon Fibre		aSe ID (% Fluorescence)
24	63.0		37.0 (93.8)
34	78.0		22.0 (76.2)
42	83.0		17.0 (52.4)
50	83.8		16.2 (32.1)

3.1.2. *Detailed studies of the relative influence of each bucky component*

To better illustrate our results, Table 3 shows the relative contribution (alongside its fluorescent energy absorption proportion) of each bucky component for the DgN values increase. Our studies shown that the contributions of each component are similar for all breast thickness considered in this work.

Our results show that breast support plate was the most influential bucky component over the DgN values increment, for all bucky models and every energy considered. This dominance can be explained by the high intensity of backscattered photons from the breast support plate that directly reach the breast surface. In addition, this component serves as an attenuating barrier for photons backscattered by the antiscatter grid and the image detector.

For a better analysis, Fig. 3 shows the influence over the DgN values with the consideration of various *BSP* models, as described in Table 1. For comparison, the influence exerted by the complete bucky (*CB1*) over the DgN is shown alongside the results. In this analysis, was considered a 2 cm thick breast.

Considering the carbon fibre *BSP* with thickness from 1.2 to 4.1 mm (Dance et al., 2000, 2009; Dance and Young, 2014), it was observed that DgN values increase linearly with thickness. This can be explained by the increase of the backscattering for thicker breast support plates. It is also observed that the DgN values estimated with the *CB1* are close to those acquired for the 4.1 mm thick *BSP*. These results are consistent with the observations of Dance et al. (2009), Dance and Young (2014) and will be further explored in Section 3.2. Comparing the results for the 2 mm *PMMA* (Massera and Tomal, 2018) and a 2 mm carbon fibre support plate (acquired through linear interpolation between 1.2 and 2.1 mm carbon fibre *BSP*), our results show that the carbon fibre support has a slightly higher influence on the DgN values. This little difference was expected due to the fact that the carbon fibre has a higher density than the *PMMA*, providing a slightly higher number of interactions suffered in this type of support.

The second most influential bucky component on DgN values was the antiscatter grid. The contribution of the *ASG* over the DgN values can be separated in two main sources: the characteristic X-rays from the radiopaque strips or cells and the backscattering from the interstitial space and the grid cover.

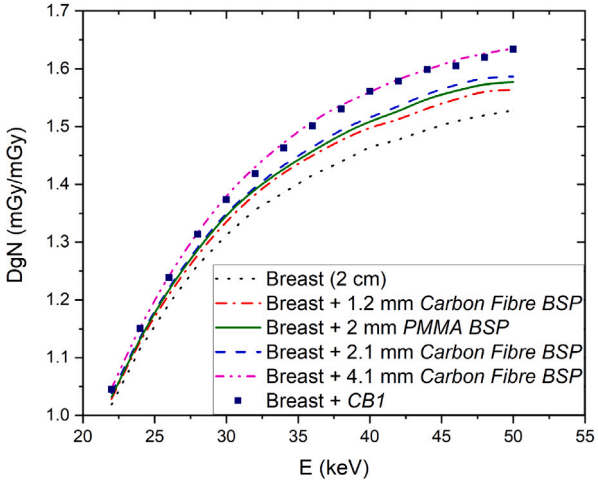

Fig. 3. DgN values as a function of the beam energy for breasts a 2 cm thick breast for the BSP models shown on Table 1 and the CB1 inclusion.

First observing the linear grid (Pb/PMMA) present on *CB1* shown in Table 3, it can be observed that for lower energies, the L_α ($\approx$ 10.54 keV) and L_β ($\approx$ 12.62 keV) fluorescent photons from the Pb strips (Sánchez Del Río et al., 2003) are the main source of the relative contribution of the linear *ASG* on DgN values due to its high production probability at lower energy, rapidly decreasing for higher beam energies. As energy increases, the backscattering from the interstitial space and the grid cover became more influential, mostly due to the increase likelihood of occurring backscattering within the PMMA interstitial space. For all energies, there was no relevant contribution on DgN values from the backscattering on the lead strips.

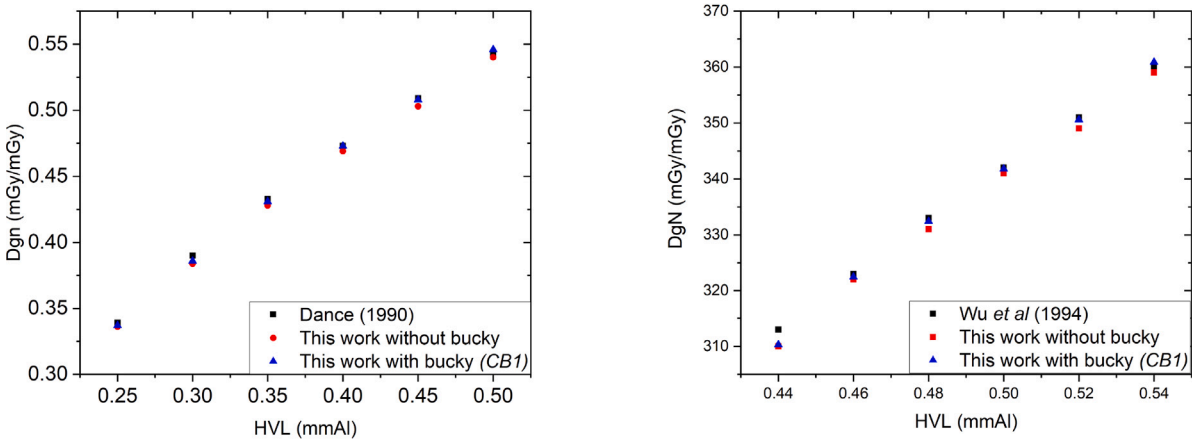

(a) (b)

Fig. 4. Comparison between DgN values as a function of half-value layer (HVL) for the geometric model and simulation conditions proposed by Dance (1990) (2 cm thick breast) and Wu et al. (1994) (3 cm thick breast), with and without the inclusion of a bucky (*CB1*). In addition, the DgN values obtained by the authors are presented.

Now observing the cellular grid (Cu/air) present on *CB2* shown in Table 3, the Cu fluorescence photons from the cells exerted little contribution to the overall antiscatter grid influence on DgN values. This was expected due the relatively low energy of the copper K_α (≈ 8.04 keV) and K_β (≈ 8.91 keV) fluorescent photons (Sánchez Del Río et al., 2003). This low energy is highly attenuated on the way to the breast tissue, and become less likely to occur as the energy increases. Although in this case, it was observed that the copper strips have a increase of backscattering for higher energies. For all energies, the contribution from the interstitial space (air) backscattering was irrelevant.

The least influential component was the image detector for all energies considered and systems simulated. For both detectors present on *CB1* and *CB2*, this low influence was expected due to the presence of the *ASG* that blocks the majority of the emerging photons from the detector. From Table 3, it is observed that the CsI detector only exerted a little contribution on the *CB1* overall influence for energies above 34 keV, due the characteristic X-rays from the detector. Now observing the aSe detector present on *CB2*, it is observed that its influence is negligible for all energies. This little influence decreases even more with the increasing energy, due the decrease of the probability of fluorescence photons to occur. Tests carried out without the antiscattering grid (*CB3*) showed that the relative contribution of the aSe detector greatly increases, reaching 37% of the total influence on DgN increment for 24 keV beam. However as seen previously, the detector contribution decreases for higher energies, due the decrease of the fluorescence production.

3.2. Studies carried out with geometric models and simulation conditions provided by literature

3.2.1. The minimal influence of bucky inclusion on DgN values for studies with conventional beams

Fig. 4 shows the simulated DgN values for conditions and geometric models proposed by Dance (1990) and Wu et al. (1994) for a 2 and 3 cm thick breast, respectively.

For both comparisons shown in Fig. 4, the bucky inclusion on the geometric model exerted minimal influence over DgN values (less than 1.0%). Nevertheless, a slight discrepancy between the results with and without the bucky inclusion is observed for higher HVL. This is expected due to the increase of the mean energy of the beam and it is an indicator of how the bucky presence can affect the DgN values when high-energy spectra is considered.

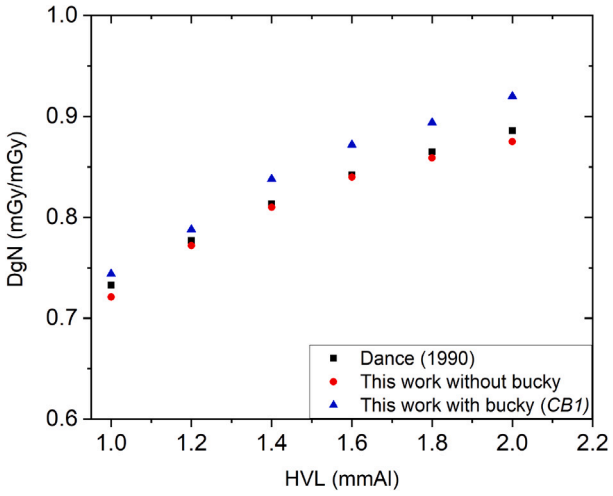

Fig. 5. Simulated DgN values in this work with and without the inclusion of a complete bucky (CB1) model, using the methodologies and geometric models proposed by Dance (1990), for a 2 cm thick breast with 50% glandular fraction.

3.2.2. The importance of the bucky consideration for studies with high-energy beams

Fig. 5 shows the simulated DgN values for the conditions and geometric models proposed by Dance (1990), with and without the inclusion of a bucky (*CB1*), followed by the literature results. The simulations were performed using the high-energy mammography spectra (W/Al) described in Table 2. A 2 cm thick breasts was considered.

Fig. 5 shows the bucky influence on DgN values increasing with HVL. For HVLs of 1.0 and 2.2 mmAl, the bucky inclusion increased the DgN values by 3.1 and 5.1%, respectively. High-energy beams have greater transmission ratio in thinner breasts. In addition, due to the higher energies that compose these spectra, it is expected that a larger number of photons backscatter on the bucky, causing the observed increase of their influence on DgN values in comparison to conventional (low-energy) beams.

To analyse the influence of kVp over the bucky influence on the DgN, additional tests were carried out using various spectra (W/Al) with tube potentials between 40 and 50 kV and fixed HVL at 2.2 mmAl. The bucky influence on DgN values remained practically unchanged, varying up to 0.2%. This observation shows that the bucky influence

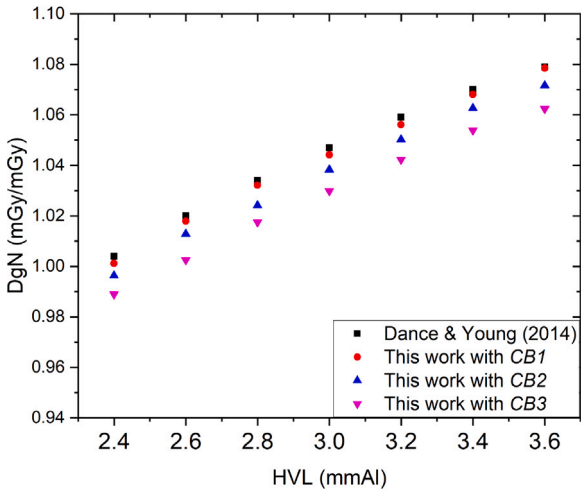

Fig. 6. Simulated DgN values for the methodology proposed by Dance and Young (2014), accurately reproducing its geometric model with a 4.1 mm carbon fibre, or using bucky models proposed in Table 1. DgN values were computed for a 4 cm thick breasts with 50% glandular fraction.

over the DgN depends strongly on spectra HVL and mean energy, but minimally on kVp.

Since the simulation of a complete bucky can be complex and time demanding, a solution would be the substitution of the whole components for a homogeneous carbon fibre block placed right under the breast, as previously suggested by Dance et al. (2009).

3.2.3. The variation of the influence of different bucky models on DgN values and the analysis of the consideration of a homogeneous block of carbon fibre as a substitute for simulating the complete bucky

Fig. 6 shows the simulated DgN values for the conditions and geometric models proposed by Dance and Young (2014), with the inclusion of all three complete models specified in Table 1, followed by the literature results. The simulations were performed using the high-energy mammography spectra (W/Cu) described on Table 2. A 4 cm thick breast was considered. The geometric model proposed by Dance and Young (2014) considers a 4.1 mm thick carbon fibre support. For comparison purposes, this component was replaced by the complete bucky models (*CB1*, *CB2* and *CB3*), described on Table 1. Observing Fig. 6, it is noticed that the DgN values acquired with *CB1* are in good agreement with the literature, showing similar results. However, simulations with *CB2* and *CB3* which have less influential components (cellular grid for only *CB2* and aSe detector), presented smaller DgN values (up to 1.5%) if compared with the literature.

Our tests showed that consideration of a 4.1 mm thick carbon fibre block in simulations can replace a complete bucky model similar to *CB1*, in agreement with the literature (Dance et al., 2009; Dance and Young, 2014). Although the literature recommendation can overestimate the influence of other bucky models. Additional tests showed that the bucky models *CB2* and *CB3* can be accurately replaced by a 4 mm and 3.9 mm thick carbon fibre blocks, respectively.

4. Conclusion

The tests carried out with monoenergetic beams showed that implementation of the bucky in the geometric model can be relevant for *DgN* acquisitions that considers thinner breasts and X-ray energies higher than 24 keV. The *DgN* was more influenced by the breast support plate for all considered geometric models, being responsible by up to 60% of the total increase of *DgN* values, depending on which model was adopted. The antiscatter grid showed a minor, although noticeable influence on the *DgN* increment. The image detector showed a small importance on the results, being relevant only for geometric models that do not consider the antiscatter grid.

Tests carried out with polyenergetic beams showed that the consideration of the bucky on the acquisition of *DgN* is highly recommended when high-energy mammography X-ray spectra is considered, which can be relevant on the application of advanced mammographic techniques, such as contrast-enhanced mammography. To reduce the time of simulation of DgN values and simplify the geometric models considered, it was observed that the whole bucky can be substituted by a homogeneous carbon fibre block with thickness between 3.9 and 4.1 mm, depending on its components.

Many studies have shown that the energy deposition in glandular tissues can change with its distribution (Oliver and Thomson, 2019) and how the *MGD* and *DgN* can drastically change if compared with homogeneous breast models (Hernandez et al., 2015; Chang et al., 2020; Ferrauche et al., 2023; Sechopoulos et al., 2023). Therefore, there is a necessity to expand the studies towards heterogeneous breast models.

CRediT authorship contribution statement

J. Godeli: Writing – original draft, Visualization, Validation, Project administration, Methodology, Investigation, Formal analysis, Data curation, Conceptualization. **D.M. Cunha:** Writing – review & editing, Validation, Investigation, Data curation. **M.P.A. Potiens:** Resources, Project administration, Funding acquisition. **M.E. Poletti:** Writing – review & editing, Visualization, Validation, Supervision, Resources, Project administration, Investigation, Funding acquisition, Conceptualization.

Declaration of competing interest

The authors declare the following financial interests/personal relationships which may be considered as potential competing interests: Julio Godeli Neto reports financial support was provided by Coordination of Higher Education Personnel Improvement. Martin Eduardo Poletti reports financial support was provided by National Council for Scientific and Technological Development. Maria da Penha Albuquerque Potiens reports financial support was provided by State of Sao Paulo Research Foundation. If there are other authors, they declare that they have no known competing financial interests or personal relationships that could have appeared to influence the work reported in this paper.

Data availability

Data will be made available on request.

Acknowledgements

The author acknowledges the partial financial support received from Coordination for the Improvement of Higher Education Personnel (CAPES), the National Council for Scientific and Technological Development (CNPq) (Grant Numbers: 312643/2018-7 and 311710/2022-0) and the São Paulo Research Foundation (FAPESP) (Grant Number: 2018/05982-0).

References

AAPM, 2015. Monte Carlo Reference Data Sets for Imaging Research *The Report of AAPM Task Group 195*. Technical Report, American Association of Physicists in Medicine.

ACR, 1999. Quality Control Manual Mammography. Technical Report, American College of Radiology.

ACR, 2018. Digital Mammography Quality Control Manual. Technical Report, American College of Radiology.

Almansa, J., Salvat-Pujol, F., Diaz-Londoño, G., Carnicer, A., Lallena, A., Salvat, F., 2021. PENGEOM – A general-purpose geometry package for Monte Carlo simulation of radiation transport in complex material structures (new version announcement). Comput. Phys. Comm. 264, 107962.

Boone, J., 1999. Glandular breast dose for monoenergetic and high-energy X-ray beams: Monte Carlo assessment. Radiology 203, 23–37.

Boone, J.M., 2002. Normalized glandular dose (DgN) coefficients for arbitrary X-ray spectra in mammography: Computer-fit values of Monte Carlo derived data. Med. Phys. 29 (April), 869–875.

Boone, J.M., Fewell, T.R., Jennings, R.J., 1997. Molybdenum, rhodium, and tungsten anode spectral models using interpolating polynomials with application to mammography. Med. Phys. 24 (12), 1863–1874.

Carlsson, G.A., Dance, D., 1992. Breast absorbed doses in mammography: Evaluation of experimental and theoretical approaches. Radiat. Prot. Dosim. 43 (1–4), 197–200.

Chang, T., Lai, K., Tu, C., Wu, J., 2020. Three-layer heterogeneous mammographic phantoms for Monte Carlo simulation of normalized glandular dose coefficients in mammography. Sci. Rep. 10.

Cunha, D.M., Tomal, A., Poletti, M.E., 2012. Optimization of X-ray spectra in digital mammography through Monte Carlo simulations. Phys. Med. Biol. 57 (7), 1919–1935.

Cunha, D.M., Tomal, A., Poletti, M.E., 2013. Monte Carlo simulation of X-Ray spectra in mammography and contrast-enhanced digital mammography using the code PENELOPE. IEEE Trans. Nucl. Sci. 60 (2), 495–502.

Dance, D.R., 1990. Monte Carlo calculation of conversion factors for the estimation of mean glandular breast dose. Phys. Med. Biol. 35 (9), 1211–1219.

Dance, D.R., Hunt, R.A., Bakic, P.R., Maidment, A.D., Sandborg, M., Ullman, G., Carlsson, G.A., 2005. Breast dosimetry using high-resolution voxel phantoms. Radiat. Prot. Dosim. 114 (1–3), 359–363.

Dance, D.R., Persliden, J., Carlsson, G.A., 1992. Calculation of dose and contrast for two mammographic grids. Phys. Med. Biol. 37 (1), 235–248.

Dance, D.R., Sechopoulos, I., 2016. Dosimetry in X-ray-based breast imaging. Phys. Med. Biol. 61 (19), R271–R304.

Dance, D.R., Skinner, C.L., Carlsson, G.A., 1999. Breast dosimetry. Appl. Radiat. Isot. 50 (1), 185–203.

Dance, D.R., Skinner, C.L., Young, K.C., Beckett, J.R., Kotre, C.J., 2000. Additional factors for the estimation of mean glandular breast dose using the UK mammography dosimetry protocol. Phys. Med. Biol. 45 (11), 3225–3240.

Dance, D.R., Young, K.C., 2014. Estimation of mean glandular dose for contrast enhanced digital mammography: Factors for use with the UK, European and IAEA breast dosimetry protocols. Phys. Med. Biol. 59 (9), 2127–2137.

Dance, D., Young, K., Engen, R., 2011. Estimation of mean glandular dose for breast tomosynthesis: Factors for use with the UK, European and IAEA breast dosimetry protocols. Phys. Med. Biol. 56, 453–471.

Dance, D.R., Young, K.C., Van Engen, R.E., 2009. Further factors for the estimation of mean glandular dose using the United Kingdom, European and IAEA breast dosimetry protocols. Phys. Med. Biol. 54 (14), 4361–4372.

Del Lama, L.S., Godeli, J., Poletti, M.E., 2017. Monte Carlo simulation studies for the determination of microcalcification thickness and glandular ratio through dual-energy mammography. Radiat. Phys. Chem. 137, 157–162.

Ding, H., Molloi, S., 2017. Quantitative contrast-enhanced spectral mammography based on photon-counting detectors: A feasibility study. Med. Phys. 44 (8), 3939–3951.

Engen, R., Bosmans, H., Dance, D.R., Heid, P., Lazzari, B., Marshall, N., Schopphoven, S., Thijssen, M., Young, K., 2013. Digital Mammography Update, European Protocol for the Quality Control of the Physical and Technical Aspects of Mammography Screening, fourth ed. European Commission, Luxembourg.

Fedon, C., Longo, F., Mettivier, G., Longo, R., 2015. GEANT4 for breast dosimetry: Parameters optimization study. Phys. Med. Biol. 60 (16), 311–323.

Fedon, C., Rabin, C., Caballo, M., Diaz, O., Garcia, E., Rodríguez-Ruiz, A., González-sprinberg, G.A., Sechopoulos, I., 2019. Monte Carlo study on optimal breast voxel resolution for dosimetry estimates in digital breast tomosynthesis. Phys. Med. Biol. 64 (1), 1–23.

Ferrauche, G., Tramontin, G., Massera, R.T., Tomal, A., 2023. Impact of fibroglandular tissue distribution and breast shape in voxelized breast models for dosimetry in mammography. Phys. Med. Biol. 68 (7), 074003.

Hammerstein, G.R., Miller, D.W., White, D.R., Masterson, M.E., Woodard, H.Q., Laughlin, J.S., 1979. Absorbed radiation dose in mammography. Radiology 130 (2), 485–491.

Hemdal, B., 2011. Forward-scattered radiation from the compression paddle should be considered in glandular dose estimations. Radiat. Prot. Dosim. 147 (1–2), 196–201.

Hernandez, A.M., Seibert, J.A., Boone, J.M., 2015. Breast dose in mammography is about 30% lower when realistic heterogeneous glandular distributions are considered. Med. Phys. 42 (11), 6337–6348.

Higgins, P.D., Attix, F.H., Hubbell, J.H., Seltzer, S.M., Berger, M.J., Sibata, C.H., 1991. Mass Energy Transfer and Mass Energy Absorption Coefficients, Including Inflight Positron Annihilation for Photon Energies 1-keV to 100-MeV. Technical Report, National Inst. of Standards and Technology.

Huang, S.Y., Boone, J.M., Yang, K., Kwan, A.L., Packard, N.J., 2008. The effect of skin thickness determined using breast CT on mammographic dosimetry. Med. Phys. 35 (4), 1199–1206.

IAEA, 2007. Dosimetry in Diagnostic Radiology: An International Code of Practice. Technical Report, IAEA, Viena.

ICRU, 2016. Key data for ionizing-radiation dosimetry: Measurements standards and applications (ICRU Report 90). J. Int. Comm. Radiat. Units Meas. 14 (1), NP.

IPEM, 2005. The commissioning and routine testing of mammographic X-ray systems. Technical Report, IPEM, York.

Karlsson, M., Nygren, K., Wickman, G., Hettinger, G., 1976. Absorbed dose in mammary radiography. Acta Radiol. Therapy Phys. Biol. 15 (3), 252–258.

Massera, R.T., Tomal, A., 2018. Skin models and their impact on mean glandular dose in mammography. Phys. Medica 51 (January), 38–47.

Miglioretti, D., Lange, J., van den Broek, J., Lee, C., van Ravesteyn, N., Ritley, D., Kerlikowske, K., Fenton, J., Melnikow, J., de Koning, H., Hubbard, R., 2016. Radiation-Induced breast cancer incidence and mortality from digital mammography screening: A modeling study. Ann. Intern. Med. 164 (4), 205–214.

Nosratieh, A., Hernandez, A., Shen, S.Z., Yaffe, M.J., Seibert, J.A., Boone, J.M., 2016. Mean Glandular dose coefficients (DgN) for X-ray spectra used in contemporary breast imaging systems. Phys. Med. Biol. 60 (18), 7179–7190.

Oliver, P.A.K., Thomson, R.M., 2019. Investigating energy deposition in glandular tissues for mammography using multiscale Monte Carlo simulations. Med. Phys. 46 (3), 1426–1436.

Rezentes, P.S., De Almeide, A., Barnes, G.T., 1999. Mammography grid performance. Radiology 210 (1), 227–232.

Salvat, F., Fernández-Varea, J.M., Sempau, J., 2009. PENELOPE, a Code System for Monte Carlo Simulation of Electron and Photon Transport. Technical Report, NUCLEAR ENERGY AGENCY no. 6416, Paris, France, p. 339.

Sánchez Del Río, M., Brunetti, A., Golosio, B., Simionovici, A., 2003. XRAYLIB tables (X-Ray fluorescence cross-section). Europ. Synchrotron Radiat. Facil. Univ. Sassari 188.

Sarno, A., Dance, D.R., Van Engen, R.E., Young, K.C., Russo, P., Di Lillo, F., Mettivier, G., Bliznakova, K., Fei, B., Sechopoulos, I., 2017. A Monte Carlo model for mean glandular dose evaluation in spot compression mammography:. Med. Phys. 44 (7), 3848–3860.

Sechopoulos, I., Ali, E.S., Badal, A., Badano, A., Boone, J.M., Kyprianou, I.S., Mainegra-Hing, E., McMillan, K.L., McNitt-Gray, M.F., Rogers, D.W., Samei, E., Turner, A.C., 2015. Monte Carlo reference data sets for imaging research: Executive summary of the report of AAPM Research Committee Task Group 195. Med. Phys. 42 (10), 5679–5691.

Sechopoulos, I., Dance, D.R., Boone, J.M., Bosmans, H.T., Caballo, M., Diaz, O., van Engen, R., Fedon, C., Glick, S.J., Hernandez, A.M., Hill, M.L., Hulme, K.W., Longo, R., Rabin, C., Sanderink, W.B.G., Seibert, J.A., 2023. Joint AAPM task group 282/EFOMP working group report: Breast dosimetry for standard and contrast-enhanced mammography and breast tomosynthesis. Med. Phys. 51 (2), 712–739.

Sechopoulos, I., Suryanarayanan, S., Srinivasan, V., D'Orsi, C.J., Karellas, A., 2007. Scatter radiation in digital tomosynthesis of the breast. Med. Phys. 34 (2), 564–576.

Stanton, L., Villafana, T., Day, J.L., Lightfoot, D.A., 1984. Dosage evaluation in mammography. Radiology 150, 577–584.

Sung, H., Ferlay, J., Siegel, R.L., Laversanne, M., Soerjomataram, I., Jemal, A., Bray, F., 2021. Global cancer statistics 2020: GLOBOCAN estimates of incidence and mortality worldwide for 36 cancers in 185 countries. CA: Cancer J. Clin. 71 (3), 209–249.

Wilkinson, L., Heggie, J.C.P., 2001. Glandular breast dose: Potential errors. Radiology 213 (October), 1.

Wu, X., Barnes, T., Tucker, M., 1991. Spectral dependence of glandular tissue dose in screen-film mammography. Radiology 179 (1), 143–148.

Wu, X., Gingold, E.L., Barnes, G.T., Tucker, D.M., 1994. Normalized average glandular dose in molybdenum target-rhodium filter and rhodium target-rhodium filter mammography.. Radiology 193, 83–89.

Yaffe, M.J., 2010. Detectors for digital mammography. In: Bick, U., Diekmann, F. (Eds.), Digital Mammography. Springer Berlin Heidelberg, pp. 13–31, Chapter 2.

Zhang, D., Li, X., Liu, B., 2012. X-ray spectral measurements for tungsten-anode from 20 to 49 kVp on a digital breast tomosynthesis system. Med. Phys. 39 (6), 3493–3500.

Zhao, B., Zhao, W., 2008. Imaging performance of an amorphous selenium digital mammography detector in a breast tomosynthesis system. Med. Phys. 35 (5), 1978–1987.

Zhou, A., Yin, Y., White, G., Davidson, R., 2016. A new solution for radiation transmission in anti-scatter grids. Biomed. Phys. Eng. Express 2, 055011.